Published OnlineFirst October 20, 2017; DOI: 10.1158/0008-5472.CAN-17-2105

Molecular and Cellular Pathobiology

Cancer Research

SGK1 Is a Critical Component of an AKT-Independent Pathway Essential for PI3K-Mediated Tumor Development and Maintenance

Arturo Orlacchio[1], Michela Ranieri[1], Martina Brave[1], Valeria Antico Arciuch[1], Toni Forde[1], Daniela De Martino[1], Karen E. Anderson[2], Phillip Hawkins[2], and Antonio Di Cristofano[1]

Abstract

Activation of the PI3K–AKT signaling cascade is a common critical event during malignant transformation. In this study, we used thyroid gland epithelial cells and a series of genetically engineered mouse strains as model systems to demonstrate that, although necessary, AKT activation is not sufficient for PI3K-driven transformation. Instead, transformation requires the activity of the PDK1-regulated AGC family of protein kinases. In particular, SGK1 was found to be essential for proliferation and survival of thyroid cancer cells harboring PI3K-activating mutations. Notably, cotargeting SGK1 and AKT resulted in significantly higher growth suppression than inhibiting either PI3K or AKT alone. Overall, these findings underscore the clinical relevance of AKT-independent pathways in tumors driven by genetic lesions targeting the PI3K cascade. *Cancer Res; 77(24); 6914–26. ©2017 AACR.*

Introduction

Activation of PI3K signaling through a variety of mechanisms, including *PIK3CA*-activating mutations or amplification, and *PTEN* mutation, deletion, or silencing, is found in about 40% of all human cancers (1, 2). Some specific tumor types, such as breast, prostate, colorectal, and endometrial cancer, as well as glioblastoma and anaplastic thyroid carcinoma, show even higher mutation rates for members of this pathway (2, 3). PI3K-dependent generation of phosphatidylinositol-3,4,5-triphosphate (PIP3) triggers membrane recruitment of proteins containing a PH-domain, such as the three AKT isoforms and the PDK1 kinase. Furthermore, it leads to the activation of the mTORC2 complex by relieving an autoinhibitory mechanism involving its component, SIN1 (4). mTORC2 and PDK1 act then in concert to phosphorylate and activate AKT (5, 6).

Although, traditionally, AKT is considered the primary effector of PI3K-transforming activity, there is accumulating evidence that additional PI3K-dependent pathways may play a critical role during neoplastic transformation (7) or in driving adaptive resistance to PI3K inhibition (8, 9).

In fact, mTORC1 and mTORC2, two key PI3K effectors, activate, in cooperation with PDK1, several members of the AGC family of kinases, including S6K, PKC, and SGK (10). These targets, in turn, are known to control pathways with direct bearing on the transformation process (11).

In view of these notions, it is noteworthy that a formal, systematic *in vivo* genetic approach to address the questions of (i) whether AKT activation is sufficient for tumor development and maintenance, and (ii) what is the role in these processes, if any, of the other PI3K/PDK1–dependent pathways, has never been reported.

As PI3K activation is a common feature of advanced and aggressive thyroid cancer (3), we have used the thyroid gland as a relevant model system to address this issue and have generated a series of mouse models in which different critical components of the PI3K signaling cascade have been selectively manipulated in the thyroid epithelial cells.

We have found that although AKT activation is essential for PI3K-dependent neoplastic transformation, it is clearly not sufficient. In fact, we show that activation of PDK1-dependent AGC kinases is essential for tumor development. Furthermore, we provide evidence that the AGC kinase family member SGK1 plays a critical role downstream of PI3K activation for tumor maintenance and that it represents a critical therapeutic target.

Materials and Methods

Animals

The *Pten*$^{thyr-/-}$, [*Pten*$^{thyr-/-}$,*Kras*^{G12D}], and [*Pten,Tp53*]$^{thyr-/-}$ strains have been described previously (12–14). *Pdk1*^{L155E} mice (15) were kindly provided by Dr. Dario Alessi (University of Dundee, Dundee, Scotland). All strains were backcrossed in the 129S6/SvEv background for at least 10 generations. All experimental procedures involving mice were conducted in accordance with IACUC-approved protocols.

[1]Department of Developmental and Molecular Biology, Albert Einstein College of Medicine, Bronx, New York. [2]Inositide Laboratory, Babraham Institute, Babraham, Cambridge, United Kingdom.

Note: Supplementary data for this article are available at Cancer Research Online (http://cancerres.aacrjournals.org/).

Current address for V. Antico Arciuch: Institute of Biological Chemistry-CONICET, School of Sciences, University of Buenos Aires, Argentina.

Corresponding Author: Antonio Di Cristofano, Department of Developmental and Molecular Biology, Albert Einstein College of Medicine, 1301 Morris Park Avenue, Price 302, Bronx, NY 10461. Phone: 718-678-1137; Fax: 718-678-1020; E-mail: antonio.dicristofano@einstein.yu.edu

doi: 10.1158/0008-5472.CAN-17-2105

©2017 American Association for Cancer Research.

Downloaded from cancerres.aacrjournals.org on November 1, 2021. © 2017 American Association for Cancer Research.

Published OnlineFirst October 20, 2017; DOI: 10.1158/0008-5472.CAN-17-2105

Tissue analysis

Formalin-fixed samples were paraffin embedded and processed for routine hematoxylin and eosin staining. Six-micron sections were subjected to antigen retrieval, incubated with antibodies against Ki67 (Dako), and counterstained with hematoxylin.

Alternatively, mice were injected intraperitoneally with bromodeoxyuridine (BrdUrd; 10 mg/kg, Sigma) 2 hours before sacrifice. Anti-Ki67 and anti–BrdUrd-stained sections were analyzed using the ImageJ software.

Western blot analysis and antibodies

Cells, thyroids, and tumor tissue were homogenized on ice in RIPA buffer (Thermo Fisher Scientific) supplemented with Halt Protease and Phosphatase Inhibitor cocktail (Thermo Fisher Scientific). Protein concentration was determined using the Pierce BCA Protein Kit (Thermo Fisher Scientific). Western blot analysis was carried out using 30 to 50 μg proteins run on Bis-Tris SDS precast gels (GenScript).

All the primary antibodies used were purchased from Cell Signal Technology and used at a dilution of 1:1,000 in 5% BSA in TBS-T. Signals were detected with HRP-conjugated secondary antibodies (Thermo Fisher Scientific) and the chemiluminescence substrate Luminata Crescendo (EMD Millipore). Equivalent loading was confirmed with anti–β-actin (Sigma-Aldrich).

Cell lines, drug treatments, and cell proliferation

Cell lines were established from tumors developed in $Pten^{thyr-/-}$, $[Pten,\ Tp53]^{thyr-/-}$ and $[Pten^{thyr-/-}, Kras^{G12D}, Pdk1^{L155E}]$ mice as described previously (16, 17). All mouse cell lines, as well as the human cell lines 8505c, ACT1, and CAL62 were grown in DMEM (HyClone) supplemented with 10% FBS (HyClone) and Mycozap Plus-CL (Lonza Biologics). The human cell lines TAD2, N-Thy-Ori, T235, T238, THJ21T, SW1736, C643, Ocut2, T243, and THJ16T were grown in RPMI (HyClone) supplemented with 10% FBS (HyClone) and Mycozap Plus-CL. All cell lines were maintained at 37°C with 5% CO_2. Cell identity was validated by STS profiling as well as by amplifying and sequencing genomic fragments encompassing their known mutations.

Chemical inhibitors GSK650394, EMD638683, MK2206, and GDC-0941 were purchased from Selleck Chemicals and dissolved in DMSO.

For drug sensitivity experiments on parental cell lines, all inhibitors were added 24 hours after plating. After 72 hours of treatment, cells were detached and counted using a Z2 Coulter counter (Beckman Coulter). Final DMSO concentration in media was always below 0.1%. EC_{50} value calculation and statistical analysis were done using GraphPad Prism (GraphPad Software).

In experiments on lentivirally transduced cell lines, cells were pretreated with 250 ng/mL (THJ16T) or 500 ng/mL (T4888M) doxycycline hyclate (Sigma-Aldrich) for 48 hours prior to treatment with GDC-0941. Drugs were added immediately after cell seeding.

For long-term doubling rate experiments, 5×10^4 cells were plated in the presence of chemical inhibitors or doxycycline hyclate. Every 3 days, cells were harvested, counted, and 5×10^4 cells were reseeded.

Statistical analysis of drug synergy was evaluated from the results of the Wst-1 assays and calculated using the Chou–Talalay method (18) and the CalcuSyn Software (Biosoft). To determine synergy between two drugs, the software uses a median-effect method that determines whether the drug combination produces greater effects together than expected from the summation of their individual effects. The combination index (CI) values are calculated for the different dose-effect plots (for each of the serial dilutions) based on the parameters derived from the median-effect plots of the individual drugs or drug combinations at the fixed ratios. The CI was calculated on the basis of the assumption of mutually nonexclusive drug interactions. CI values significantly >1 are antagonistic, not significantly different than 1 are additive, and values <1 are synergistic.

3D spheroid assays

A total of 5×10^3 cells were plated in 96-well round bottom, ultralow attachment plates (Corning). Spheroid volume was measured after 3 and 10 days using ImageJ.

shRNAs and doxycycline-inducible cell lines

Cells were transduced with lentiviruses encoding shRNAs against *SGK1* (from the TRC Genome-Wide shRNA Collection). After preliminary experiments with a battery of previously fully validated clones (9), shRNA TRCN0000040175 was chosen for subsequent experiments due to its superior targeting efficiency.

ShRNA TRCN0000040175 was cloned into the Tet-pLKO-puro (Addgene plasmid #21915). Lentiviral constructs were packaged in HEK293 cells transfected using Lipofectamine 2000 (Invitrogen). Viral supernatant was collected 48 to 72 hours after transfection, combined, and filtered using 0.45-μm Nalgene SFCA syringe filters (Thermo Fisher Scientific). Target cells were plated 24 hours before infection and then exposed to viral supernatant supplemented with 20 μg/mL polybrene (Santa Cruz Biotechnology). Mouse cell lines were then selected for at least 72 hours with puromycin (Corning) 5 μg/mL, whereas a concentration of 2 μg/mL was used for human cell lines.

Transduced cell lines were pretreated with 250 to 500 ng/mL doxycycline hyclate for 48 hours prior to plating for growth curve experiments. After seeding, cells were counted every 24 hours, and cell number was determined as described previously. In all experiments performed on transduced cell lines, doxycycline hyclate was replaced every 24 hours.

PIP3 determination

Mass spectrometry was used to measure inositol lipid levels essentially as described previously (19), using a QTRAP 4000 (AB Sciex) mass spectrometer and employing the lipid extraction and derivitization method described for whole tissue, with the modification that frozen tissue samples were ground under liquid N2 with a mortar and pestle prior to analysis (instead of Dounce homogenizer), and that 10 ng C17:0/C16:0 PtdIns(3,4,5)P_3 ISD (internal standard) and 10 ng C17:0/C16:0 PtdIns ISD was added to primary extracts. Final samples were dried in a speedvac concentrator rather than under N2. Measurements were conducted in triplicate per experiment, 0.5 mg per sample.

RNA extraction and real-time PCR

Total RNA was extracted with TRIzol reagent (Invitrogen) according to the manufacturer's protocol. RNA yields were assessed using a NanoDrop 1000 (Thermo Fisher Scientific). RNA (1 μg) was reverse transcribed using the Maxima First Strand cDNA Synthesis Kit (Thermo Fisher Scientific) according to the manufacturer's instructions. qRT-PCR was conducted on a StepOne Plus apparatus using the Absolute Blue qPCR Rox Mix (Thermo Fisher Scientific) and TaqMan expression assays

Downloaded from cancerres.aacrjournals.org on November 1, 2021. © 2017 American Association for Cancer Research.

Published OnlineFirst October 20, 2017; DOI: 10.1158/0008-5472.CAN-17-2105

(Applied Biosystem) following the manufacturer's instructions. The TaqMan expression assays used were Mm00441380_m1 (Sgk1), Mm00449845_m1 (Sgk2), Mm00453797_m1 (Sgk3), Mm02026778_g1 (Akt2), and Mm00446973_m1 (Tbp). Each sample was run in triplicate, and Akt2 and Tbp were used to normalize the input RNA. Relative quantities were calculated using the $2^{-\Delta\Delta C_t}$ method.

Cell-cycle DNA analysis

Transduced cell lines were seeded in 10-cm plates, cultured overnight at 37°C, and incubated for 72 hours with doxycycline hyclate 250 ng/mL. Cells were harvested by trypsin treatment and fixed in 70% ethanol in ice for 30 minutes. After treatment with RNase (Genentech/Roche) for 5 minutes at room temperature, cells were stained with propidium iodide (Genentech/Roche) overnight, and DNA content was measured using a BD *FACSCanto II* system (BD Biosciences).

Annexin V staining

Cell lines were seeded in 100-mm plates, cultured overnight at 37°C, and incubated for 72-96-120 hours with doxycycline hyclate. Cells were harvested by trypsinization, and supernatant was also collected. Cells were stained with Annexin V FITC and propidium iodide (BD Biosciences) for 15 minutes at room temperature in the dark. Samples were analyzed by flow cytometry within 1 hour using a BD *FACSCanto II* system (BD Biosciences). Flow cytometry analysis was performed on the FloJo platform.

In vivo experiments

Eight-week-old NSG mice, from the Einstein Shared Facility in Stem Cell Research, were injected subcutaneously with 5×10^6 T4888M or THJ16T cells previously transduced with an inducible shRNA targeting *SGK1*. When tumors reached a size between 100 and 150 mm^3, mice were randomized to control and doxycycline hyclate treatment groups. Doxycycline hyclate was dissolved in water and administered via oral gavage (100 mg/kg) daily, and tumor volume was calculated from two-dimensional measurements using the equation: tumor volume = (length × width^2) × 0.5. Tumor weight was measured at the end of the experiment.

Results

AKT activation is indispensable for PI3K-dependent transformation

Pten$^{thyr-/-}$ mice are born with mildly hyperplastic thyroid glands (12) and slowly develop solid, nodular lesions that progress to locally invasive follicular carcinomas after one year of age (Fig. 1A and B; ref. 20). To test to what extent unrestrained PI3K relies on AKT activation to induce hyperproliferation and transformation of mouse thyrocytes, we generated a mouse model in which *Akt1* and *Akt2* are simultaneously deleted in the thyroid epithelial cells, alone or in combination with the loss-of-function *Pten* allele. *Akt3* was excluded from this analysis, as its expression is undetectable in the mouse thyroid (Supplementary Fig. S1).

Although codeletion of *Akt1* and *Akt2* did not cause any overt phenotype, and did not alter thyroid size or histology at any time point analyzed, it drastically inhibited the development of both follicular hyperplasia and nodular lesions in *Pten*$^{thyr-/-}$ mice (no triple-mutant mice with nodules at 48 weeks, vs. 66.7% of *Pten*$^{thyr-/-}$ mice; Fig. 1A and B).

Thus, based on *in vivo* genetic data, AKT activation appears to be an absolute requirement for the oncogenic activity of unrestrained PI3K. It remains to be seen, however, whether it is sufficient to drive thyrocyte transformation.

Notably, we found that the size of the thyroid in the triple mutants was still slightly but significantly larger than that of wild-type mice (Fig. 1A), suggesting that AKT is not the only player downstream of active PI3K to participate in the thyroid hyperplastic response.

Also AGC kinase activation is essential for PI3K-dependent transformation

In addition to AKT, PI3K controls, via mTORC1 and mTORC2, the activation of several members of the AGC family of protein kinases, including S6K, SGK, and a number of PKC isoforms (10). Similar to AKT, activation of these kinases requires two phosphorylation events, one in the activation loop, mediated by PDK1, and the other in the hydrophobic motif, mediated by mTORC1 or mTORC2. Other AGC kinases such as RSK, instead, require ERK1/2 activity for the hydrophobic motif phosphorylation. In stark contrast with AKT, phosphorylation of the AGC kinase activation loop is absolutely dependent on prior phosphorylation of the hydrophobic motif, which creates a docking site for the PIF-pocket of PDK1 (21). Consequently, a point mutation in the PIF-pocket, L155E, completely abolishes PDK1 ability to activate all the AGC kinases, without impacting its ability to phosphorylate AKT (22).

We have taken advantage of this differential activation mechanism to explore the role and relevance of AGC kinases activation downstream of PI3K.

To this end, *Pten*$^{thyr-/-}$ mice were crossed to mice in which the *Pdk1* L155E-mutant allele is expressed from its endogenous locus in a Cre-dependent manner (15). The resulting compound mutant progeny was then compared with sex- and age-matched wild-type and single-mutant mice. Western blot analysis of thyroid extracts confirmed that AKT was still fully phosphorylated in the double mutants and was able to phosphorylate its targets, GSK3α/β, while the PIF pocket–dependent S6K was, as predicted, unable to phosphorylate ribosomal protein S6 (Fig. 1C).

Analysis of control, *Pten*$^{thyr-/-}$, and compound mutant mice at 12, 48, and 60 weeks of age revealed that impairment of AGC kinase activation significantly mitigates the hyperplastic phenotype observed in the thyroid of *Pten*$^{thyr-/-}$ mice. Both thyroid weight and thyrocyte proliferative index were reduced by at least 50% at each time point analyzed, strongly suggesting that AKT activation is only partially responsible for the hyperproliferative phenotype, and that AGC kinase-driven pathways are critical for thyroid proliferation (Fig. 1D–F).

Histologic analysis of these thyroids revealed striking differences: at 48 weeks of age, when over 60% of *Pten*$^{thyr-/-}$ female mice display nodular lesions, and a few of them (3%) already have progressed to invasive carcinomas, 97% of *Pten*$^{thyr-/-}$,*Pdk1*^{L155E} compound mutant mice displayed only mild hyperplasia (Fig. 2A and B). At 60 weeks, when over 46% of *Pten*$^{thyr-/-}$ female mice display invasive carcinomas, and 43% have nodular lesions, 94% of *Pten*$^{thyr-/-}$,*Pdk1*^{L155E} compound mutant mice still displayed simple hyperplasia (Fig. 2A and B). We have previously reported (20) that male *Pten*$^{thyr-/-}$ mutants show a delay in the development of thyroid neoplastic lesions. At 60 weeks of age, 7% of *Pten*$^{thyr-/-}$ male mice display invasive carcinomas, and 64% have

Downloaded from cancerres.aacrjournals.org on November 1, 2021. © 2017 American Association for Cancer Research.

Published OnlineFirst October 20, 2017; DOI: 10.1158/0008-5472.CAN-17-2105

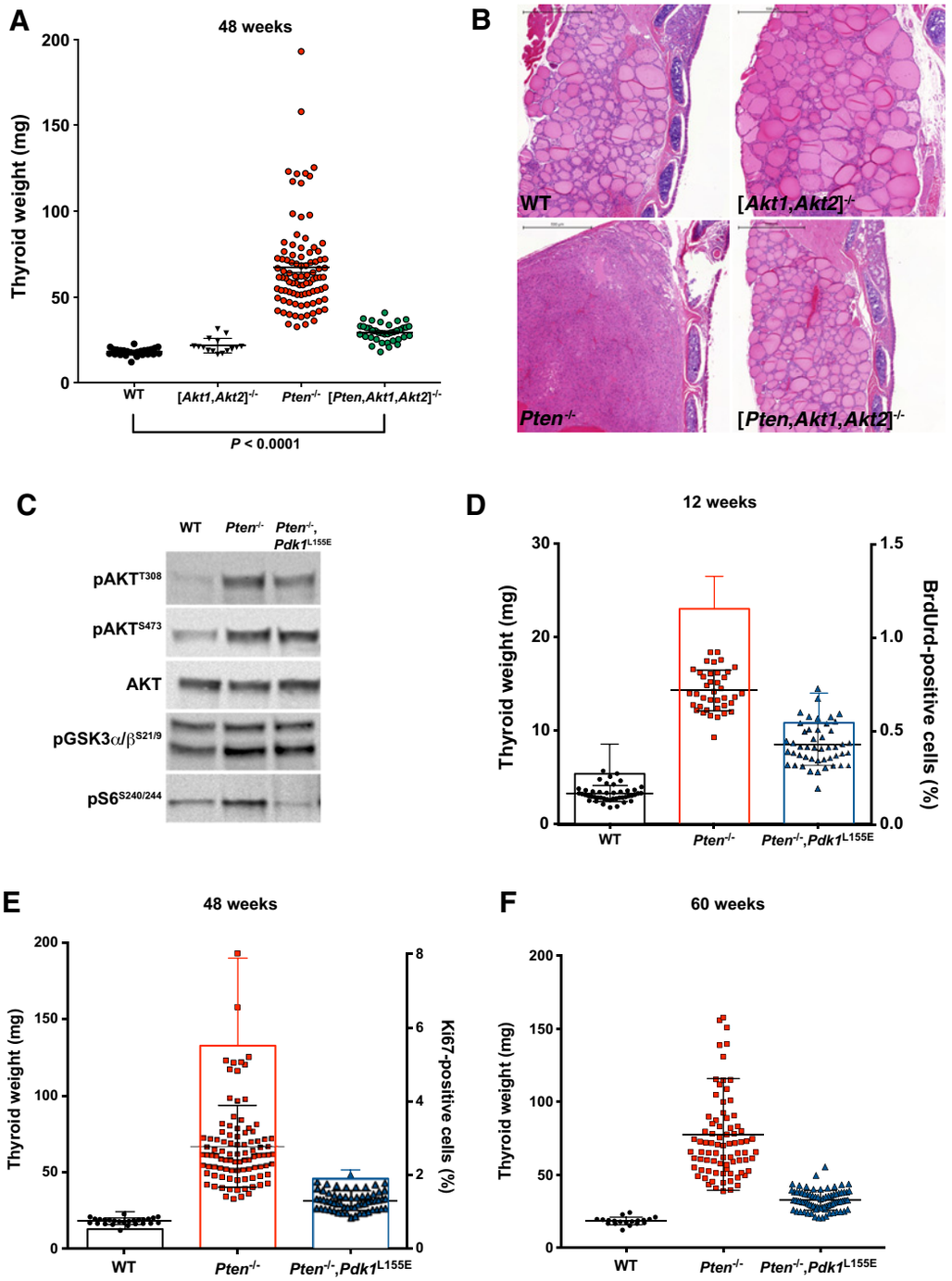

Figure 1.

Genetic analysis of the role of AKT and PDK1-dependent AGC kinases in the development of thyroid hyperplasia. **A,** Thyroid weight at 48 weeks of age for mice of the indicated genotypes. **B,** Hematoxylin and eosin staining of representative sections from thyroid glands dissected from 48-week old mice of the indicated genotypes. Bar, 500 μm. **C,** Western blot analysis showing that the *Pdk1* L155E allele does not affect AKT phosphorylation and activity, but completely impairs the activity of the PIF pocket–dependent AGC kinase S6K. **D–F,** Thyroid weight at 12, 48, and 60 weeks of age, showing the effect of the *Pdk1* L155E allele on the hyperplasia induced by *Pten* deletion. In addition, the thyroid proliferative index was measured by BrdUrd incorporation (**D**) or by Ki67 staining (**E**).

nodular lesions; on the other hand, 94% of $Pten^{thyr-/-}$,$Pdk1^{L155E}$ compound mutant males displayed simple hyperplasia (Supplementary Fig. S2). These data strongly suggest that, despite constitutive AKT activity, the simple thyroid hyperplasia developed by $Pten^{thyr-/-}$,$Pdk1^{L155E}$ compound mutants does not progress to neoplastic lesions.

Downloaded from cancerres.aacrjournals.org on November 1, 2021. © 2017 American Association for Cancer Research.

Published OnlineFirst October 20, 2017; DOI: 10.1158/0008-5472.CAN-17-2105

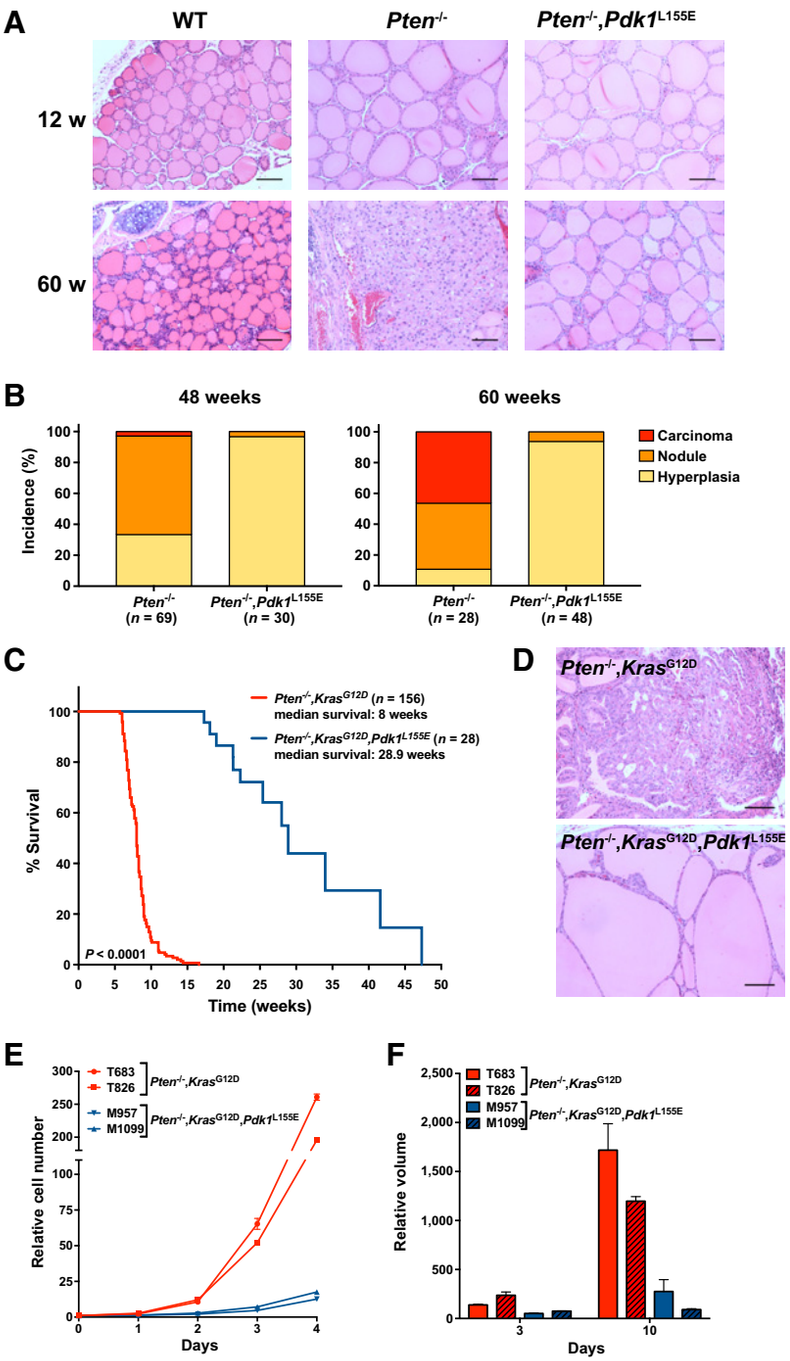

Figure 2.

The *Pdk1* L155E allele prevents PI3K-dependent tumor development. **A,** Hematoxylin and eosin staining of representative sections from thyroid glands dissected from 12- and 60-week old mice of the indicated genotypes. Bar, 100 μm. **B,** Effect of the *Pdk1* L155E allele on the incidence of hyperplasia, solid nodules, and carcinomas in *Pten*$^{thyr-/-}$ mice at 48 and 60 weeks of age. **C,** Kaplan–Meier analysis of the effect of the *Pdk1* L155E allele on the survival of *Pten*$^{thyr-/-}$,*Kras*^{G12D} mice. **D,** Hematoxylin and eosin staining of representative sections from thyroid glands dissected from mice of the indicated genotypes, showing that the *Pdk1* L155E allele prevents the development of solid, invasive tumors. **E,** Analysis of the effect of the *Pdk1* L155E allele on the proliferation of cell lines established from thyroid glands dissected from mice of the indicated genotypes. **F,** 3D growth analysis of spheroids derived from the same cell lines as in **E**. Size is expressed as final volume at day 7 divided by the initial volume measured at 24 hours after plating.

AGC kinase inactivation drastically impairs tumor progression in aggressive models of thyroid cancer

The thyroid lesions developed by *Pten*$^{thyr-/-}$ mice progress very slowly to invasive tumors. This prompted us to analyze the effect of ablating AGC kinase activation in more aggressive models of thyroid cancer. We have reported that simultaneous thyroid-specific activation of Kras and PI3K leads to the rapid development of aggressive carcinomas (14). When we introduced the *Pdk1* L155E-mutant allele into this strain, we found that the median survival of the triple compound mutants was increased from 8 to 29 weeks (Fig. 2C). Furthermore, histologic analysis revealed that the lesions developed by the triple mutants were not solid carcinomas, as in the *Pten*$^{thyr-/-}$,*Kras*^{G12D} mice, but rather massive hyperplasias ultimately leading to mouse death via airway compression (Fig. 2D).

We have generated stable cell lines from thyroid lesions developed by *Pten*$^{thyr-/-}$,*Kras*^{G12D} (20) as well as by *Pten*$^{thyr-/-}$, *Kras*^{G12D},*Pdk1*^{L155E} mice. In agreement with the *in vivo* data, cell lines carrying the *Pdk1* L155E-mutant allele proliferated dramatically slower than their *Pdk1* wild-type counterpart, both in

Downloaded from cancerres.aacrjournals.org on November 1, 2021. © 2017 American Association for Cancer Research.

Published OnlineFirst October 20, 2017; DOI: 10.1158/0008-5472.CAN-17-2105

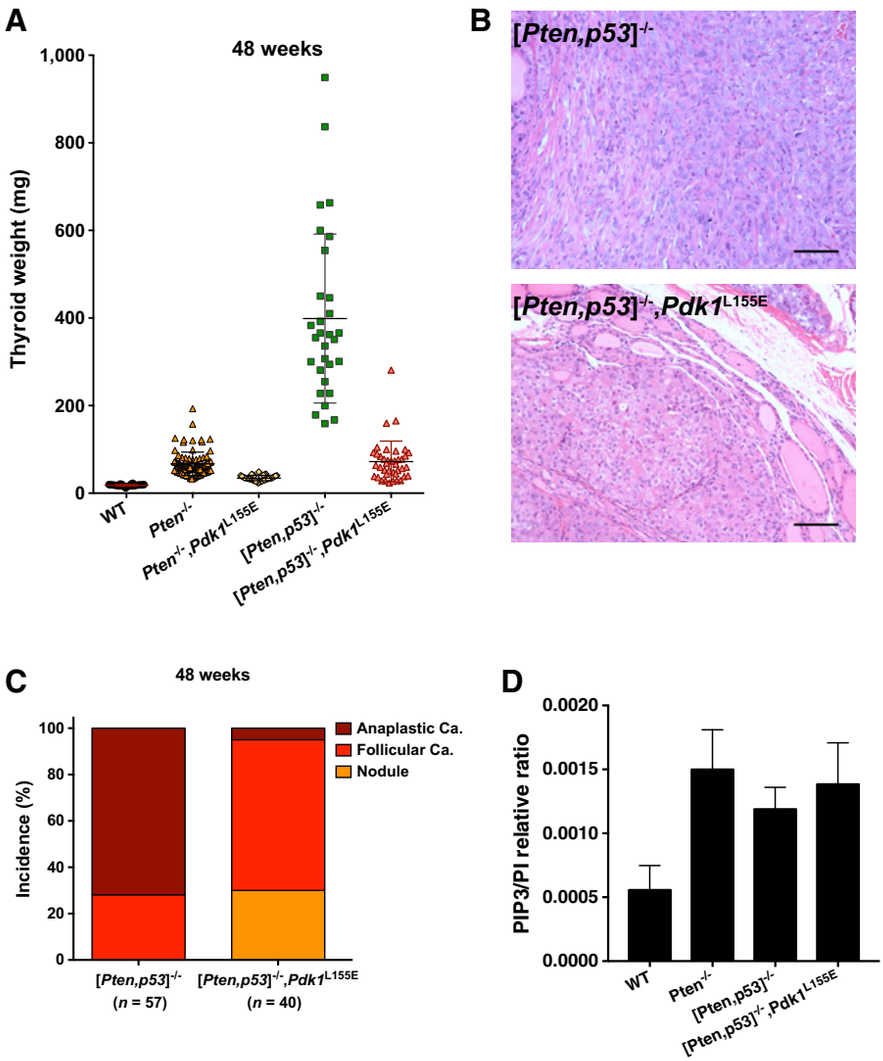

Figure 3.
The *Pdk1* L155E allele prevents the development of anaplastic carcinomas in [*Pten, Tp53*]$^{thyr-/-}$ mice. **A,** Thyroid weight at 48 weeks of age for mice of the indicated genotypes. **B,** Hematoxylin and eosin staining of representative sections from thyroid glands dissected from mice of the indicated genotypes, showing that the *Pdk1* L155E allele prevents the development of undifferentiated tumors. **C,** Effect of the *Pdk1* L155E allele on the incidence of solid nodules, follicular, and anaplastic carcinomas in [*Pten, Tp53*]$^{thyr-/-}$ mice at 48 weeks of age. **D,** Mass spectrometry measurement of the PIP3/PI ratio in extracts from thyroids of the indicated genotypes.

standard culture conditions and as spheroids in the more physiologic 3D growth conditions (Fig. 2E and F).

Finally, we tested the effect of the *Pdk1* L155E-mutant allele on the development of anaplastic thyroid carcinoma, the most aggressive and undifferentiated subtype of thyroid cancer, using the [*Pten, Tp53*]$^{thyr-/-}$ model (16). [*Pten, Tp53*]$^{thyr-/-}$ mice develop follicular carcinomas early on, which progress to anaplastic carcinomas in over 70% of cases by 48 weeks of age.

Impairment of AGC kinase activation reduced the weight of the compound mutant glands by 75%, to the same level observed in single-mutant *Pten*$^{thyr-/-}$ mice (Fig. 3A). Histologic analysis of these lesions showed that only 5% of cases had nests of undifferentiated cells, while 65% of cases showed only well-differentiated follicular carcinomas, and 30% nodular hyperplasia (Fig. 3B and C).

Thus, despite constitutive PI3K and AKT activation, neoplastic lesions developed by [*Pten, Tp53*]$^{thyr-/-}$, *Pdk1*^{L155E} thyroids are unable to progress to aggressive, undifferentiated anaplastic carcinomas.

Genetic manipulation of PI3K downstream effectors might lead to unexpected feedbacks that could impact PI3K catalytic activity. To assess the activation status of PI3K in our genetic models, we measured the levels of phosphatidylinositol-3,4,5-triphosphate (PIP3) in wild-type, single, double, and triple mutant thyroids, using a well-established mass spectrometry approach and found that PIP3 levels were increased, as expected, in *Pten*$^{thyr-/-}$ mice, but did not change upon introduction of additional mutant alleles (Fig. 3D).

Thus, despite a fully active PI3K/AKT axis, *Pten*$^{thyr-/-}$ thyrocytes absolutely need AGC kinase activity to reach their full transformation potential, which is dictated by the additional genetic alterations introduced (*Kras, Tp53*, etc.).

Activation of SGK family members is required for PI3K-active cancer cell proliferation

To identify the critical AGC kinase that is required for full PI3K oncogenic activity, we used a large panel of mouse and human thyroid cancer cell lines encompassing the spectrum of mutations most commonly found in advanced thyroid tumors and performed a sensitivity screen using small-molecule inhibitors of PI3K and mTORC1 (as controls), and of the PI3K-regulated AGC kinase families, S6K, PKC, and SGK.

Downloaded from cancerres.aacrjournals.org on November 1, 2021. © 2017 American Association for Cancer Research.

Published OnlineFirst October 20, 2017; DOI: 10.1158/0008-5472.CAN-17-2105

Strikingly, we found that PKC and S6K inhibitors had little to no effect on the proliferation of thyroid cancer cells at concentrations commonly used in cell culture assays. On the other hand, GSK650394, an SGK inhibitor, had a dramatic growth-suppressive effect, especially in cells carrying driver mutations that activate PI3K signaling (Fig. 4A).

Given the lack of antibodies specifically recognizing active SGK, we tested the phosphorylation level of NDRG1, a bona fide SGK target, in the thyroids of wild-type, *Pten*-mutant, and double-mutant mice, and found that, indeed, SGK activation is increased in $Pten^{thyr-/-}$ thyroids and returns at baseline levels in the glands of $Pten^{thyr-/-}$,$Pdk1^{L155E}$ compound mutant mice (Fig. 4B).

These data suggest that SGK is the critical AGC kinase that is required for PI3K full oncogenic activity.

Commercially available SGK inhibitors are notoriously suboptimal in terms of target selectivity. To verify that SGK is indeed the critical target affecting thyroid cancer cell proliferation, we first reduced the dose of GSK650394 by 40% and found that a 3 μmol/L concentration was still able to profoundly inhibit proliferation of PI3K-active cell lines (Fig. 4C). Then we compared the response of nine thyroid cancer cell lines to both GSK650394 (3 μmol/L) and to another SGK inhibitor, EMD638686, again used at a lower concentration (2.5 μmol/L) than usually found in published studies (10 μmol/L). We found a strong correlation between the sensitivity of these cells to the two inhibitors, further suggesting that they are indeed targeting SGK (Fig. 4D).

Next, we used the four $Pten^{-/-}$,$Kras^{G12D}$ cell lines described above, two of which also carry the $Pdk1^{L155E}$ mutation, to demonstrate that these two inhibitors were able to decrease cell proliferation in a dose-dependent manner in the AGC kinase-proficient cells, but not in the AGC kinase-defective lines (Fig. 4E and F). Furthermore, we tested whether GSK650394 could affect the ability of SGK to phosphorylate NDRG1 in T4888M cells and found that it significantly reduced NDRG1 phosphorylation. Interestingly, concomitant AKT inhibition was required for full ablation of phosphorylation, suggesting that, at least in specific cellular contexts, NDRG1 is a common target of SGK and AKT (Fig. 4G).

Finally, we performed a time course analysis of the effect of 3 μmol/L GSK650394 on the proliferation of PI3K-active thyroid cancer cells and found that SGK inhibition profoundly affected cell growth, with inhibition rates ranging between 63% and 95% after 4 days (Fig. 4H), thus formally validating SGK as a critical component of the PI3K-dependent oncogenic machinery.

SGK1 depletion reduces proliferation and viability of PI3K-active cancer cells

SGK is a family of three closely related kinases. To assess their relative contribution to the transformation process, we analyzed the RNA level of the three isoforms in the thyroid of control, *Pten*-mutant, and double-mutant mice and found that *Sgk1* is the most highly expressed of the three genes, while *Sgk2* expression levels are several orders of magnitude lower than those of *Sgk1* and *Sgk3* (Fig. 5A). These results were also confirmed at the protein level, in thyroid extracts from wild-type and *Pten*-mutant mice (Fig. 5B). More variability, instead, was observed in mouse thyroid cancer cell lines, where, although *Sgk1* is still the most expressed gene, the relative expression of *Sgk2* and *Sgk3* is different in each line (Fig. 5C). The almost undetectable expression of *Sgk2* suggests that this isoform is unlikely to play a critical role in the control of thyroid cell proliferation. On the other hand, *Sgk3* is unique among the SGK genes, as it has an N-terminal PX-domain targeting the protein to the endosomes, where it is activated in response to the class III PI3K Vps34 (23). On the basis of these notions, as well as on preliminary shRNA-based experiments showing very limited effects of *Sgk3* depletion on cell proliferation (Supplementary Fig. S3), we focused on *Sgk1* as the primary conduit of this AKT-independent, PI3K-driven pathway.

Preliminary experiments revealed that constitutive and sustained shRNA-mediated *Sgk1* depletion is not tolerated by PI3K-active thyroid cancer cells and that no stably transduced pools could be maintained for more than a few passages. Thus, we generated doxycycline-inducible mouse and human thyroid cancer cell lines, using a previously validated shRNA (9) that targets both mouse and human *SGK1* (Fig. 5D). Four days of *SGK1* depletion resulted in reduced NDRG1 phosphorylation and in a slight increase in AKT activation, accompanied by a minor increase in GSK3β phosphorylation (Fig. 5D). However, no changes in S6 phosphorylation were observed.

Analysis of cell proliferation upon sh*Sgk1* induction revealed dramatic growth suppression in both mouse (Fig. 5E–G) and human (Fig. 5H) thyroid cancer cells harboring driver mutations that activate PI3K signaling, with inhibition rates ranging between 68% and 98% after 6 days of doxycycline treatment. The growth-suppressive effect, conversely, was significantly lower in human thyroid cancer cell lines without mutations activating PI3K (44%; Fig. 5I; Supplementary Fig. S4).

Flow cytometric analysis of control and sh*Sgk1*-induced thyroid cancer cells showed that SGK depletion caused arrest in G_1 at early time points (Fig. 5J), followed, 24 to 48 hours later, by induction of a significant degree of apoptosis (Fig. 5K).

Taken together, these data show that PI3K-active thyroid cancer cells absolutely need SGK1 activity to support sustained proliferation and survival.

To test the long-term effect of SGK1 depletion on the growth of PI3K-active thyroid cancer cells, we performed a 3-week long analysis of cell proliferation using the THJ16T cell line. Induction of sh*SGK1* drastically reduced cell proliferation, which reached its lowest level by day 6 and then remained rather constant for the remainder of the follow-up (Fig. 6A). SGK1-depleted cells, however, did not undergo irreversible growth inhibition or senescence, as doxycycline removal after 12 days promptly restored the normal proliferation rate for these cells (Fig. 6A, green line).

SGK1 depletion impairs tumor growth *in vivo*

To test the effect of SGK1 depletion on tumor growth *in vivo*, we generated xenograft models using the murine T4888M cell line ($Pten^{-/-}$, $Tp53^{-/-}$) and the human THJ16T cell line ($PIK3CA^{E545K}$, $TP53^{-/-}$). Doxycycline-mediated induction of the shRNA targeting SGK1 severely impaired tumor growth in both models (Fig. 6B and C). In line with the higher knockdown level (see Fig. 5D), the effect was more dramatic in the THJ16T xenograft: SGK1 depletion resulted in tumor regression in almost 90% of cases, with complete tumor disappearance in 25% of the mice (Fig. 6D). These results were further validated by tumor weight analysis at endpoint, demonstrating that, despite continuous PI3K signaling, SGK1 depletion reduced mean tumor size by over 80% (Fig. 6E).

IHC analysis of these tumors showed no significant changes in the number of apoptotic cells. However, the fraction of proliferating cells was strikingly reduced in SGK1-depleted cells (Fig. 6F).

Downloaded from cancerres.aacrjournals.org on November 1, 2021. © 2017 American Association for Cancer Research.

Published OnlineFirst October 20, 2017; DOI: 10.1158/0008-5472.CAN-17-2105

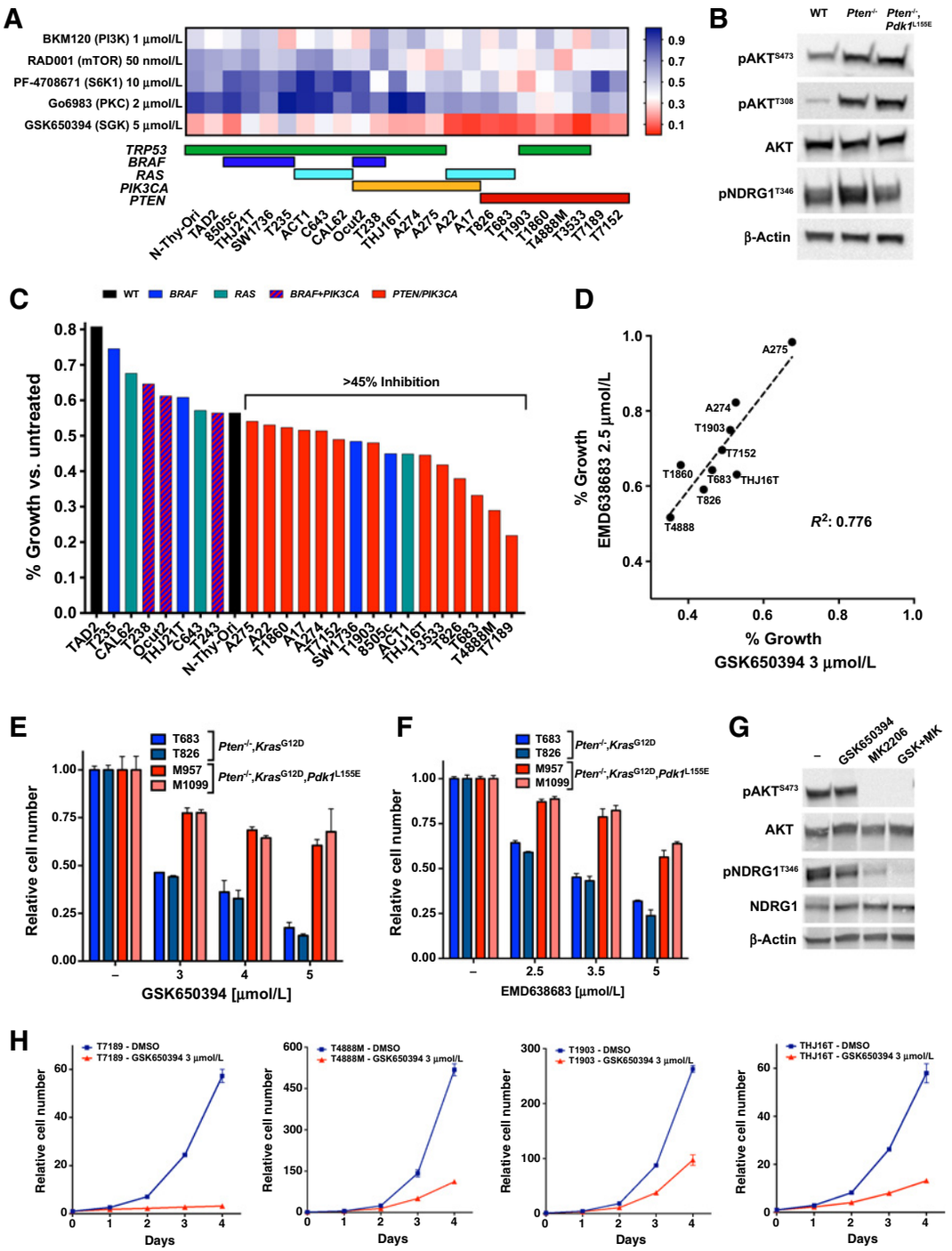

Figure 4.

SGK activity is critical for the proliferation of thyroid cancer cells carrying PI3K-activating mutations. **A,** Heatmap illustrating the effect of inhibitors of different PI3K-dependent AGC kinases on the proliferation of mouse and human thyroid cancer cell lines. Colored horizontal bars below the heatmap indicate the known driver mutation for each cell line. **B,** Western blot analysis of the phosphorylation of the SGK target, NDRG1, in the thyroids from mice of the indicated genotypes. **C,** Effect of a reduced concentration (3 μmol/L) of the SGK inhibitor GSK650394 on the proliferation of mouse and human thyroid cancer cell lines. **D,** Correlation between the responses of representative thyroid cancer cell lines to low concentrations of the SGK inhibitors GSK650394 and EMD638683. **E–F,** Differential response to two different SGK inhibitors of mouse thyroid cancer cell lines proficient or impaired in AGC kinase activation. **G,** Western blot analysis of the phosphorylation of the SGK1 target, NDRG1, in the T4888M cells upon 6-hour treatment with the indicated inhibitors. **H,** Analysis of the proliferation of different PI3K-active thyroid cancer cell lines treated with the SGK inhibitor GSK650394.

Downloaded from cancerres.aacrjournals.org on November 1, 2021. © 2017 American Association for Cancer Research.

Published OnlineFirst October 20, 2017; DOI: 10.1158/0008-5472.CAN-17-2105

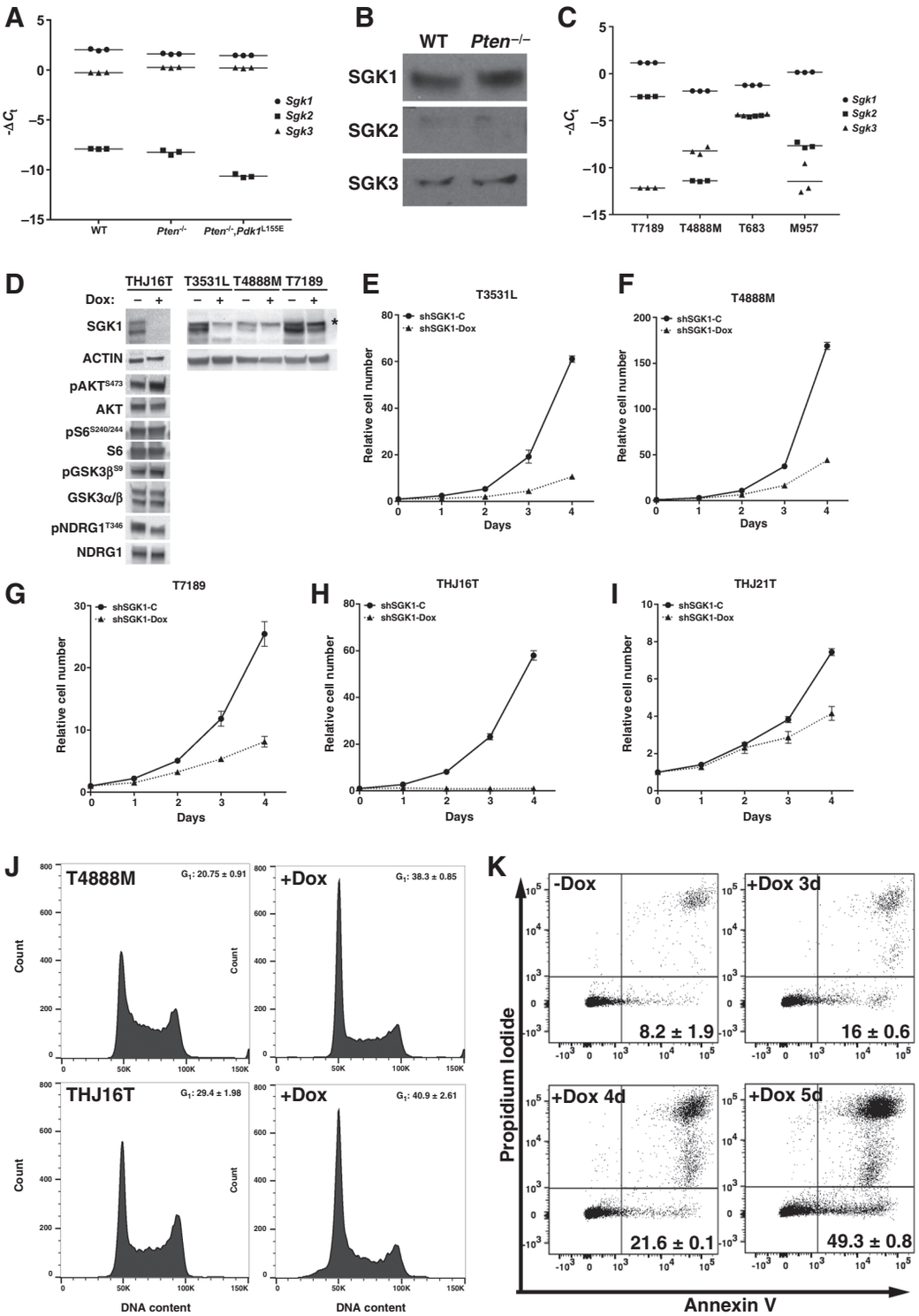

Figure 5.

SGK1 depletion impairs PI3K-dependent thyroid cancer cell proliferation. **A,** qPCR analysis of the expression of *Sgk1, -2*, and *-3* in the thyroids of mice of the indicated genotypes, showing predominant expression of *Sgk1*. **B,** Western blot validation of the qPCR results using thyroid extracts from the indicated genotypes. **C,** qPCR analysis of the expression of *Sgk1, -2*, and *-3* in mouse thyroid cancer cell lines, showing predominant expression of *Sgk1*. **D,** Western blot analysis of shRNA-mediated *SGK1* depletion upon 96-hour doxycycline treatment of the indicated cell lines. Asterisk marks a nonspecific band only observed in mouse cells. **E–H,** Analysis of the effect of doxycycline-regulated *Sgk1* depletion on the proliferation of PI3K-active mouse and human thyroid cancer cells. **I,** Representative example of the minimal effect of *SGK1* depletion on the proliferation of a human $BRAF^{V600E}$-driven thyroid cancer cell line. **J,** shRNA-mediated Sgk1 depletion induces G_1 arrest 48 hours after doxycycline treatment. **K,** shRNA-mediated Sgk1 depletion induces a time-dependent increase in apoptosis upon doxycycline treatment.

Downloaded from cancerres.aacrjournals.org on November 1, 2021. © 2017 American Association for Cancer Research.

Published OnlineFirst October 20, 2017; DOI: 10.1158/0008-5472.CAN-17-2105

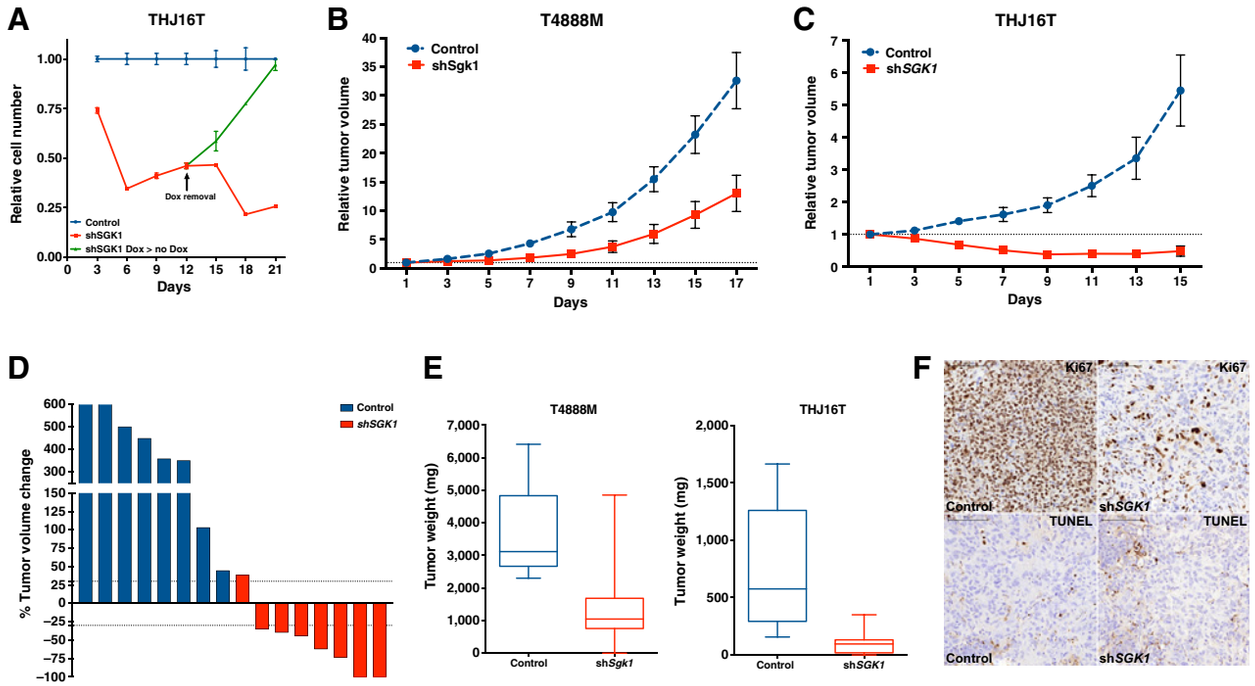

Figure 6.

SGK1 depletion impairs thyroid cancer growth *in vivo*. **A,** Long-term *Sgk1* depletion induces reversible growth suppression. A total of 50,000 THJ16T-sh*SGK1* cells were plated, then counted and replated at the same density every 3 days. **B** and **C,** T4888M-sh*Sgk1* and THJ16T-sh*SGK1* cells were injected into the flank of NSG mice; doxycycline treatment was initiated when tumors reached approximately 100 mm^3, and tumor growth was monitored every 2 days. **D,** Waterfall plot showing that *SGK1* depletion in THJ16T cells caused a 30% or more decrease in tumor size in 7 of 8 tumors. **E,** Endpoint measurement of excised tumor weight. The boxes extend from the 25th to the 75th percentiles; the line in the middle of the box is plotted at the median; the whiskers are drawn down to the 10th percentile and up to the 90th. **F,** Ki67 and TUNEL immunostaining of representative sections from control and sh*SGK1* THJ16T tumors.

SGK1 inhibition increases the efficacy of AKT targeting

The notion that SGK1 activation is fully dependent on PI3K signaling leads to the prediction that simultaneous targeting of both kinases should not result in a significant advantage over PI3K inhibition alone.

We tested this postulate using the doxycycline-inducible shSGK1 T4888M and THJ16T cell lines. As expected, the pan-PI3K inhibitor GDC0941 was clearly effective in reducing thyroid cancer cell proliferation over a 3-day period. When comparing each time point to the proliferation of untreated cells, simultaneous depletion of SGK1 dramatically increased the overall growth-suppressive effect (Fig. 7A). However, when we normalized cell proliferation at each GDC0941 concentration to the basal proliferation in the presence or absence of SGK1, thus obtaining a measure of the "net effect" of GDC0941 treatment, it became clear that SGK1 depletion paradoxically reduced the net ability of GDC0941 to inhibit cell proliferation, in particular in the THJ16T cells (Fig. 7B). These data demonstrate that SGK1 is a key PI3K downstream effector for the induction of proliferation, and thus, its absence reduces the net ability of PI3K inhibitors to impact cell proliferation, despite complete abolishment of AKT and S6 phosphorylation (Fig. 7C).

Along the same lines, simultaneous pharmacologic cotargeting of PI3K and SGKs did not result in strong synergistic activity (Supplementary Fig. S5).

Our model also predicts that targeting in combination the two major PI3K effectors, AKT and SGK, should be more effective than targeting each kinase separately. In fact, we found that the AKT inhibitor MK2206 strongly synergized with SGK inhibition in both T4888M and THJ16T cells, with a CI at EC_{90} of 0.58 and 0.45, respectively (Fig. 7C and D).

Prolonged inhibition of certain signaling pathways can elicit adaptive responses that result in the development of resistance to the inhibitor. These responses are usually not evident in the standard 3-day proliferation assays. To assess the effect of long-term pathway inhibition on cell proliferation, we measured the doubling rate of T4888M cells over a 2-week period and found that the growth-inhibitory effect of the PI3K inhibitor GDC0941, used at EC_{90}, was rapidly and progressively lost, beginning after 6 days of continuous treatment (Fig. 7E, red line). On the other hand, single-agent treatment with the AKT inhibitor MK2206 or the SGK inhibitor GSK650394, at their EC_{80}, had a more steady growth-suppressive effect. Strikingly, when administered in combination, these two inhibitors dramatically synergized, leading to almost complete inhibition of cell proliferation (Fig. 7E).

Thus, combined inhibition of the two critical PI3K effectors, AKT and SGK, has a clearly increased and prolonged therapeutic potential, compared with direct PI3K inhibition.

Discussion

Three decades of research have formally established the critical role of the PI3K/AKT/mTOR pathway in tumor development and progression (24). At the same time, the development of genetic

Downloaded from cancerres.aacrjournals.org on November 1, 2021. © 2017 American Association for Cancer Research.

Published OnlineFirst October 20, 2017; DOI: 10.1158/0008-5472.CAN-17-2105

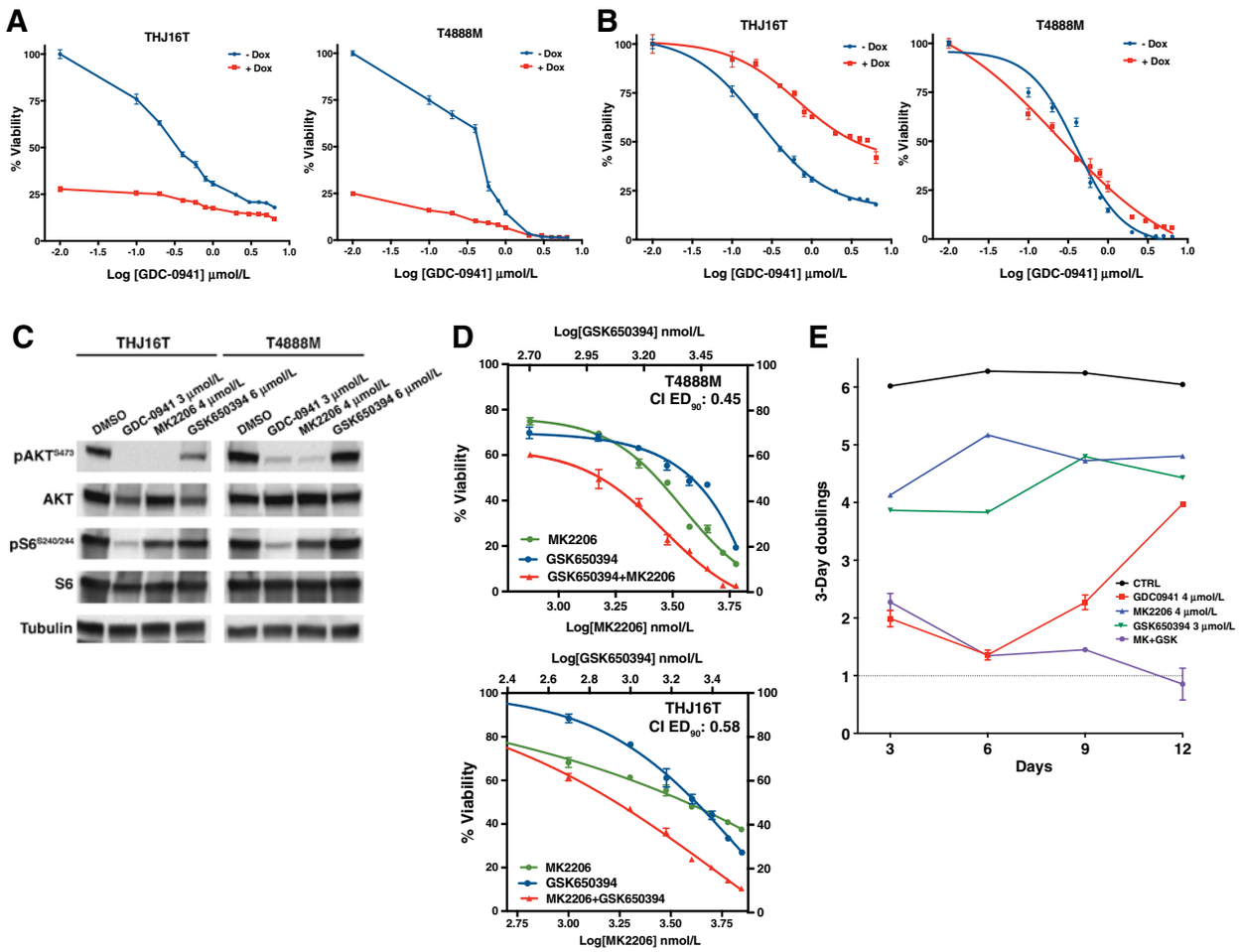

Figure 7.

Combined targeting of AKT and SGK completely inhibits proliferation of PI3K-active cancer cells. **A** and **B,** Dose–response plots showing the effect of *SGK1* depletion on the efficacy of PI3K targeting. Doxycycline + values are shown as ratio to completely untreated cells in **A** and as ratio to doxycycline-treated, GDC-0941–untreated cells in **B**. **C,** Western blot analysis of the phosphorylation of AKT and S6 in the THJ16T and T4888M cells upon 6-hour treatment with the indicated inhibitors at concentrations corresponding to EC_{75}–EC_{90} as single drug. **D,** Pharmacologic cotargeting of AKT and SGK at a constant inhibitors ratio, showing synergistic interaction between the two compounds. **E,** Long-term treatment of T4888M cells with the indicated inhibitors, showing progressive resistance to PI3K inhibition, and complete growth suppression with combined AKT and SGK inhibition.

tools for accurate pathway dissection and of small-molecule inhibitors of most members of this signaling cascade have uncovered the existence of an intricate network of signals and feedbacks, which strongly underlines the need for a deeper understanding of this pathway, if we want to effectively target it for therapeutic purposes (25).

One of the tenets that have been recently challenged by several studies is the universal role of AKT activation as the critical conduit of PI3K-transforming signals (26). As an example, activation of SGK3 has been shown to be essential for the growth of a subset of *PIK3CA*-mutant breast tumors exhibiting only minimal AKT activation (7).

Our data address for the first time, in a clinically relevant *in vivo* model, the question of AKT sufficiency in a tumor type that instead relies on AKT activity as an effector of PI3K activation. In fact, we show that simultaneous genetic ablation of *Akt1* and *Akt2* completely suppresses thyroid cancer development in mice with thyroid-specific loss of the *Pten* tumor suppressor gene, thus formally proving that AKT activity is essential for tumorigenesis downstream of PI3K in this tissue. At the same time, the residual hyperplasia observed in $[Pten, Akt1, Akt2]^{thyr-/-}$ mice suggests that additional PI3K-dependent, AKT-independent pathways contribute to thyrocyte hyperproliferation.

The *Pdk1* L155E genetic model that uncouples AKT-dependent and AKT-independent pathways downstream of PI3K has been previously utilized to show that PI3K-dependent, AKT-independent pathways are required for T-cell progenitor proliferation (27), leucine-induced mTORC1/S6K activation in the cardiac muscle (28), and proper brain patterning (29). Our data further extend these concepts by providing clear genetic evidence that activation of AGC kinases controlled by PDK1 via its PIF pocket is critical not only for the proliferative response to PI3K activation, but also for the ability of PI3K to drive neoplastic transformation and tumor progression in three well-characterized mouse models

Downloaded from cancerres.aacrjournals.org on November 1, 2021. © 2017 American Association for Cancer Research.

Published OnlineFirst October 20, 2017; DOI: 10.1158/0008-5472.CAN-17-2105

of follicular, poorly differentiated, and anaplastic thyroid cancer, respectively.

The AGC kinases cocontrolled by PI3K and PDK1 are grouped in three major families, S6K, PKC, and SGK, each with multiple members. This renders impractical any *in vivo* genetic approach to pinpoint the critical kinases that act downstream of PI3K to facilitate tumor initiation.

We elected instead to use a small-scale inhibitor-based screen, combined with shRNA approaches in established thyroid cancer cell lines, to identify which AGC kinase is required for the maintenance of the transformed phenotype in cells that depend on PI3K activity. This approach has resulted in the identification of SGK1 as the primary candidate for this role.

SGK1 was originally discovered as an immediate early gene, induced by glucocorticoids and serum (30) and has historically been associated with the control of ion transport, in particular in the kidney (31). Notably, AKT and SGK1 display a high level of target promiscuity, which has often complicated the attribution of specific functions to either of them (32). Accumulating data in recent years support the notion that SGK1 might play a distinct, AKT-independent role in cellular transformation as an effector of activated PI3K signaling. As an example, $Sgk1^{-/-}$ mice develop less colon tumors than wild-type mice when subjected to chemical carcinogenesis (33), and $Apc^{Min/+}$, $Sgk1^{-/-}$ mice display a 75% reduction in the number of tumors per mouse, compared with $Apc^{Min/+}$ mice (34).

However, the best characterized mechanism through which SGK1 has been described to contribute to transformation is via opportunistic compensation upon PI3K or AKT inhibition. In fact, in breast cancer cells expressing high levels of SGK1 and treated with a PI3K inhibitor, SGK1 was shown to stimulate mTORC1 activity by directly phosphorylating TSC2, thus inducing resistance to PI3K inhibition (8). Along the same lines, high levels of SGK1 have been found to predict resistance to AKT inhibitors in breast cancer cells (9).

Here, we have demonstrated that loss of SGK1 profoundly impacts thyroid cancer cell proliferation and survival, both *in vitro* and *in vivo*, despite intact PI3K and AKT activity. As such, our results support a new model in which SGK1 plays an essential role as an integral part of PI3K-transforming machinery.

Further in-depth work is of course warranted to identify the specific pathways controlled by SGK1 in its oncogenic role. This function might be attained by impinging upon classical AKT targets and contributing to their phosphorylation, or by controlling known SGK targets that impact cell proliferation, such as the Ca^{2+} release–activated Ca^{2+} channel (I_{CRAC}; ref. 35), potassium channels such as Kv1.3 (36), proton exchangers such as NHE3 (37), or the epithelial sodium channel, ENAC (38). Alternatively, SGK1 could phosphorylate still unknown targets, which may contribute to neoplastic transformation either directly or by controlling additional downstream players.

The notion that SGK1 is a critical component of the PI3K oncogenic pathway has obvious clinical consequences. Our data clearly show that, upon short-term exposure, SGK1 genetic depletion does not significantly increase the efficacy of PI3K inhibition, as SGK1 activation appears to be completely PI3K dependent. At the same time, however, we show that prolonged exposure to a pan-PI3K inhibitor elicits a rapid adaptive response that dramatically dampens the efficacy of the inhibitor. This effect correlates with and might be mechanistically linked to the limited and short-lived responses to different PI3K inhibitors observed in clinical trials (39–41).

Pharmacologic SGK inhibition, instead, appears to strongly cooperate with AKT inhibition, does not instigate the adaptive resistance response, and leads to sustained and powerful growth inhibition, a result of a magnitude rarely observed in anaplastic thyroid cancer models, and which might apply to additional PI3K-dependent aggressive tumor types. Of note, the absence of any major phenotype in mice lacking both *Sgk1* and *Sgk2* (42), or both *Sgk1* and *Sgk3* (43), suggests that SGK inhibition should cause limited toxicity in patients.

In conclusion, our results uncover an essential role of SGK1 in the PI3K-mediated neoplastic transformation process and warrant an increased effort in the development of small-molecule SGK inhibitors for clinical use, with the promise of more effective and long-lasting therapeutic effects.

Disclosure of Potential Conflicts of Interest

No potential conflicts of interest were disclosed.

Authors' Contributions

Conception and design: A. Orlacchio, A. Di Cristofano
Development of methodology: A. Orlacchio, V.A. Arciuch, A. Di Cristofano
Acquisition of data (provided animals, acquired and managed patients, provided facilities, etc.): A. Orlacchio, M. Ranieri, M. Brave, T. Forde, D. De Martino, K.E. Anderson, P. Hawkins
Analysis and interpretation of data (e.g., statistical analysis, biostatistics, computational analysis): A. Orlacchio, K.E. Anderson, P. Hawkins, A. Di Cristofano
Writing, review, and/or revision of the manuscript: A. Orlacchio, V.A. Arciuch, A. Di Cristofano
Administrative, technical, or material support (i.e., reporting or organizing data, constructing databases): A. Orlacchio, M. Brave
Study supervision: A. Di Cristofano

Acknowledgments

We acknowledge the Animal Housing, Histology, shRNA, Analytical Imaging, and Flow Cytometry Core Facilities of Albert Einstein College of Medicine, which are partially supported by the NIH Cancer Center Support Grant to the Albert Einstein Cancer Center (P30CA013330). This work utilized a High-Speed/Resolution Whole Slide Scanner that was purchased with funding from an NIH SIG grant 1S10OD019961-01. The Einstein Shared Facility in Stem Cell Research is supported in part by the ESSCF, NYS-DOH, Contract #C029154A. Research reported in this publication was supported by NIH grants CA172012, CA128943, and CA167839 to A. Di Cristofano.

The costs of publication of this article were defrayed in part by the payment of page charges. This article must therefore be hereby marked *advertisement* in accordance with 18 U.S.C. Section 1734 solely to indicate this fact.

Received July 13, 2017; revised September 12, 2017; accepted October 17, 2017; published OnlineFirst October 20, 2017.

References

1. Zhang Y, Kwok-Shing Ng P, Kucherlapati M, Chen F, Liu Y, Tsang YH, et al. A pan-cancer proteogenomic atlas of PI3K/AKT/mTOR pathway alterations. Cancer Cell 2017;31:820–32 e3.
2. Millis SZ, Ikeda S, Reddy S, Gatalica Z, Kurzrock R. Landscape of Phosphatidylinositol-3-kinase pathway alterations across 19784 diverse solid tumors. JAMA Oncol 2016;2:1565–73.

Downloaded from cancerres.aacrjournals.org on November 1, 2021. © 2017 American Association for Cancer Research.

Published OnlineFirst October 20, 2017; DOI: 10.1158/0008-5472.CAN-17-2105

3. Xing M. Genetic alterations in the phosphatidylinositol-3 kinase/Akt pathway in thyroid cancer. Thyroid 2010;20:697–706.
4. Liu P, Gan W, Chin YR, Ogura K, Guo J, Zhang J, et al. PtdIns(3,4,5)P3-dependent activation of the mTORC2 kinase complex. Cancer Discov 2015;5:1194–209.
5. Sarbassov DD, Guertin DA, Ali SM, Sabatini DM. Phosphorylation and regulation of Akt/PKB by the rictor-mTOR complex. Science 2005; 307:1098–101.
6. Alessi DR, James SR, Downes CP, Holmes AB, Gaffney PR, Reese CB, et al. Characterization of a 3-phosphoinositide-dependent protein kinase which phosphorylates and activates protein kinase Balpha. Curr Biol 1997;7: 261–9.
7. Vasudevan KM, Barbie DA, Davies MA, Rabinovsky R, McNear CJ, Kim JJ, et al. AKT-independent signaling downstream of oncogenic PIK3CA mutations in human cancer. Cancer Cell 2009;16:21–32.
8. Castel P, Ellis H, Bago R, Toska E, Razavi P, Carmona FJ, et al. PDK1-SGK1 signaling sustains AKT-Independent mTORC1 activation and confers resistance to PI3Kalpha inhibition. Cancer Cell 2016;30:229–42.
9. Sommer EM, Dry H, Cross D, Guichard S, Davies BR, Alessi DR. Elevated SGK1 predicts resistance of breast cancer cells to Akt inhibitors. Biochem J 2013;452:499–508.
10. Pearce LR, Komander D, Alessi DR. The nuts and bolts of AGC protein kinases. Nat Rev Mol Cell Biol 2010;11:9–22.
11. Arencibia JM, Pastor-Flores D, Bauer AF, Schulze JO, Biondi RM. AGC protein kinases: from structural mechanism of regulation to allosteric drug development for the treatment of human diseases. Biochim Biophys Acta 2013;1834:1302–21.
12. Yeager N, Klein-Szanto A, Kimura S, Di Cristofano A. Pten loss in the mouse thyroid causes goiter and follicular adenomas: insights into thyroid function and Cowden disease pathogenesis. Cancer Res 2007; 67:959–66.
13. Antico Arciuch VG, Russo MA, Dima M, Kang KS, Dasrath F, Liao XH, et al. Thyrocyte-specific inactivation of p53 and Pten results in anaplastic thyroid carcinomas faithfully recapitulating human tumors. Oncotarget 2011; 2:1109–26.
14. Miller KA, Yeager N, Baker K, Liao XH, Refetoff S, Di Cristofano A. Oncogenic Kras requires simultaneous PI3K signaling to induce ERK activation and transform thyroid epithelial cells in vivo. Cancer Res 2009;69:3689–94.
15. Bayascas JR, Sakamoto K, Armit L, Arthur JS, Alessi DR. Evaluation of approaches to generation of tissue-specific knock-in mice. J Biol Chem 2006;281:28772–81.
16. Dima M, Miller KA, Antico-Arciuch VG, Di Cristofano A. Establishment and characterization of cell lines from a novel mouse model of poorly differentiated thyroid carcinoma: powerful tools for basic and preclinical research. Thyroid 2011;21:1001–7.
17. Champa D, Russo MA, Liao XH, Refetoff S, Ghossein RA, Di Cristofano A. Obatoclax overcomes resistance to cell death in aggressive thyroid carcinomas by countering Bcl2a1 and Mcl1 overexpression. Endocr Relat Cancer 2014;21:755–67.
18. Chou TC, Talalay P. Quantitative analysis of dose-effect relationships: the combined effects of multiple drugs or enzyme inhibitors. Adv Enzyme Regul 1984;22:27–55.
19. Clark J, Anderson KE, Juvin V, Smith TS, Karpe F, Wakelam MJ, et al. Quantification of PtdInsP3 molecular species in cells and tissues by mass spectrometry. Nat Methods 2011;8:267–72.
20. Antico-Arciuch VG, Dima M, Liao XH, Refetoff S, Di Cristofano A. Cross-talk between PI3K and estrogen in the mouse thyroid predisposes to the development of follicular carcinomas with a higher incidence in females. Oncogene 2010;29:5678–86.
21. Biondi RM, Kieloch A, Currie RA, Deak M, Alessi DR. The PIF-binding pocket in PDK1 is essential for activation of S6K and SGK, but not PKB. Embo J 2001;20:4380–90.
22. Collins BJ, Deak M, Arthur JS, Armit LJ, Alessi DR. In vivo role of the PIF-binding docking site of PDK1 defined by knock-in mutation. Embo J 2003;22:4202–11.
23. Bago R, Sommer E, Castel P, Crafter C, Bailey FP, Shpiro N, et al. The hVps34-SGK3 pathway alleviates sustained PI3K/Akt inhibition by stimulating mTORC1 and tumour growth. EMBO J 2016;35:1902–22.
24. Mayer IA, Arteaga CL. The PI3K/AKT pathway as a target for cancer treatment. Annu Rev Med 2016;67:11–28.
25. Rozengurt E, Soares HP, Sinnet-Smith J. Suppression of feedback loops mediated by PI3K/mTOR induces multiple overactivation of compensatory pathways: an unintended consequence leading to drug resistance. Mol Cancer Ther 2014;13:2477–88.
26. Lien EC, Dibble CC, Toker A. PI3K signaling in cancer: beyond AKT. Curr Opin Cell Biol 2017;45:62–71.
27. Kelly AP, Finlay DK, Hinton HJ, Clarke RG, Fiorini E, Radtke F, et al. Notch-induced T cell development requires phosphoinositide-dependent kinase 1. EMBO J 2007;26:3441–50.
28. Sanchez Canedo C, Demeulder B, Ginion A, Bayascas JR, Balligand JL, Alessi DR, et al. Activation of the cardiac mTOR/p70(S6K) pathway by leucine requires PDK1 and correlates with PRAS40 phosphorylation. Am J Physiol Endocrinol Metab 2010;298:E761–9.
29. Cordon-Barris L, Pascual-Guiral S, Yang S, Gimenez-Llort L, Lope-Piedrafita S, Niemeyer C, et al. Mutation of the 3-phosphoinositide-dependent protein kinase-1 (PDK1) substrate-docking site in the developing brain causes microcephaly with abnormal brain morphogenesis independently of Akt, leading to impaired cognition and disruptive behaviors. Mol Cell Biol 2016 Sep 19. [Epub ahead of print].
30. Webster MK, Goya L, Ge Y, Maiyar AC, Firestone GL. Characterization of sgk, a novel member of the serine/threonine protein kinase gene family which is transcriptionally induced by glucocorticoids and serum. Mol Cell Biol 1993;13:2031–40.
31. Loffing J, Flores SY, Staub O. Sgk kinases and their role in epithelial transport. Annu Rev Physiol 2006;68:461–90.
32. Di Cristofano A.SGK1: the dark side of PI3K signaling. Curr Top Dev Biol 2017;123:49–71.
33. Nasir O, Wang K, Foller M, Gu S, Bhandaru M, Ackermann TF, et al. Relative resistance of SGK1 knockout mice against chemical carcinogenesis. IUBMB Life 2009;61:768–76.
34. Wang K, Gu S, Nasir O, Foller M, Ackermann TF, Klingel K, et al. SGK1-dependent intestinal tumor growth in APC-deficient mice. Cell Physiol Biochem 2010;25:271–8.
35. Lang F, Shumilina E. Regulation of ion channels by the serum- and glucocorticoid-inducible kinase SGK1. FASEB J 2013;27:3–12.
36. Urrego D, Tomczak AP, Zahed F, Stühmer W, Pardo LA. Potassium channels in cell cycle and cell proliferation. Philos Trans R Soc Lond B Biol Sci 2014;369:20130094.
37. Steffan JJ, Williams BC, Welbourne T, Cardelli JA. HGF-induced invasion by prostate tumor cells requires anterograde lysosome trafficking and activity of Na+-H+ exchangers. J Cell Sci 2010;123:1151–9.
38. Liu C, Zhu LL, Xu SG, Ji HL, Li XM. ENaC/DEG in Tumor Development and Progression. J Cancer 2016;7:1888–91.
39. Sarker D, Ang JE, Baird R, Kristeleit R, Shah K, Moreno V, et al. First-in-human phase I study of pictilisib (GDC-0941), a potent pan-class I phosphatidylinositol-3-kinase (PI3K) inhibitor, in patients with advanced solid tumors. Clin Cancer Res 2015;21:77–86.
40. Doi T, Fuse N, Yoshino T, Kojima T, Bando H, Miyamoto H, et al. A Phase I study of intravenous PI3K inhibitor copanlisib in Japanese patients with advanced or refractory solid tumors. Cancer Chemother Pharmacol 2017;79:89–98.
41. Munster P, Aggarwal R, Hong D, Schellens JH, van der Noll R, Specht J, et al. First-in-human phase I study of GSK2126458, an oral pan-class I phosphatidylinositol-3-kinase inhibitor, in patients with advanced solid tumor malignancies. Clin Cancer Res 2016;22:1932–9.
42. Schnackenberg CG, Costell MH, Bernard RE, Minuti KK, Grygielko ET, Parsons MJ, et al. Compensatory role for Sgk2 mediated sodium reabsorption during salt deprivation in Sgk1 knockout mice. FASEB J 2007;21:A508.
43. Grahammer F, Artunc F, Sandulache D, Rexhepaj R, Friedrich B, Risler T, et al. Renal function of gene-targeted mice lacking both SGK1 and SGK3. Am J Physiol Regul Integr Comp Physiol 2006;290:R945–50.

Downloaded from cancerres.aacrjournals.org on November 1, 2021. © 2017 American Association for Cancer Research.

Published OnlineFirst October 20, 2017; DOI: 10.1158/0008-5472.CAN-17-2105

Cancer Research
The Journal of Cancer Research (1916–1930) | The American Journal of Cancer (1931–1940)

AACR American Association for Cancer Research

SGK1 Is a Critical Component of an AKT-Independent Pathway Essential for PI3K-Mediated Tumor Development and Maintenance

Arturo Orlacchio, Michela Ranieri, Martina Brave, et al.

Cancer Res 2017;77:6914-6926. Published OnlineFirst October 20, 2017.

Updated version	Access the most recent version of this article at: doi:10.1158/0008-5472.CAN-17-2105
Supplementary Material	Access the most recent supplemental material at: http://cancerres.aacrjournals.org/content/suppl/2017/10/20/0008-5472.CAN-17-2105.DC1

Cited articles	This article cites 42 articles, 16 of which you can access for free at: http://cancerres.aacrjournals.org/content/77/24/6914.full#ref-list-1
Citing articles	This article has been cited by 2 HighWire-hosted articles. Access the articles at: http://cancerres.aacrjournals.org/content/77/24/6914.full#related-urls

E-mail alerts	Sign up to receive free email-alerts related to this article or journal.
Reprints and Subscriptions	To order reprints of this article or to subscribe to the journal, contact the AACR Publications Department at pubs@aacr.org.
Permissions	To request permission to re-use all or part of this article, use this link http://cancerres.aacrjournals.org/content/77/24/6914. Click on "Request Permissions" which will take you to the Copyright Clearance Center's (CCC) Rightslink site.

Downloaded from cancerres.aacrjournals.org on November 1, 2021. © 2017 American Association for Cancer Research.